
Long-tail learning with attributes

Dvir Samuel¹ Yuval Atzmon² Gal Chechik^{1,2}

¹Bar-Ilan University, Ramat Gan, Israel

²NVIDIA Research, Tel Aviv, Israel

dvirsamuel@gmail.com, yatzmon@nvidia.com, gal.chechik@biu.ac.il

Abstract

Learning to classify images with unbalanced class distributions is challenged by two effects: It is hard to learn tail classes that have few samples, and it is hard to adapt a single model to both richly-sampled and poorly-sampled classes. To address few-shot learning of tail classes, it is useful to fuse additional information in the form of semantic attributes and classify based on multi-modal information. Unfortunately, as we show below, unbalanced data leads to a “familiarity bias”, where classifiers favor sample-rich classes. This bias and lack of calibrated predictions make it hard to fuse correctly information from multiple modalities like vision and attributes.

Here we describe DRAGON, a novel modular architecture for long-tail learning designed to address these biases and fuse multi-modal information in face of unbalanced data. Our architecture is based on three classifiers: a vision expert, a semantic attribute expert that excels on the tail classes, and a debias-and-fuse module to combine their predictions. We present the first benchmark for long-tail learning with attributes and use it to evaluate DRAGON. DRAGON outperforms state-of-the-art long-tail learning models and Generalized Few-Shot-Learning with attributes (GFSL-a) models. DRAGON also obtains SoTA in some existing benchmarks for single-modality GFSL.

1 Introduction

Learning with unbalanced data is challenging yet wide-spread. In most fields and domains, few classes (or types) are commonly observed, while the (many) remaining ones are rarely encountered. This long-tail distribution is consistently found across many fields: In text documents, Zipf’s law states that the frequency of words decays inversely with their rank; With acoustic noise, the power spectrum tends to decay as $1/f$; In visual object recognition, the distribution of classes has a long tail [31]. Surprisingly, learning with long-tail data was little explored until recently, perhaps because many research datasets are artificially balanced.

Long-tail data poses two major challenges to learning: *data paucity* and *data imbalance*. First, at the tail of the distribution, classes are poorly sampled, and one has to use few-shot and zero-shot learning techniques. The second issue is *data imbalance*. When training a single model for both richly-sampled classes and poorly-sampled classes, models over-represent the rich classes in terms of model parameters. To put it simply, common classes dominate the loss during optimization, and as a result, models devote more of their representation capacity to the rich-sampled classes. Learning with unbalanced data poses a fundamental algorithmic problem because classical learning theory asserts that model capacity should grow with the number of samples.

To address *data paucity* for classes at the tail, one can supplement the visual examples with prior information about classes. This information can be given as text or attributes [16, 24, 3, 37]. This approach, *learning with attributes* has been studied mostly for zero-shot and generalized zero-shot learning [26, 21]. Here we propose to adapt it to few-shot learning by fusing information from two modalities. A visual classifier that is trained on visual samples and designed to classify correctly

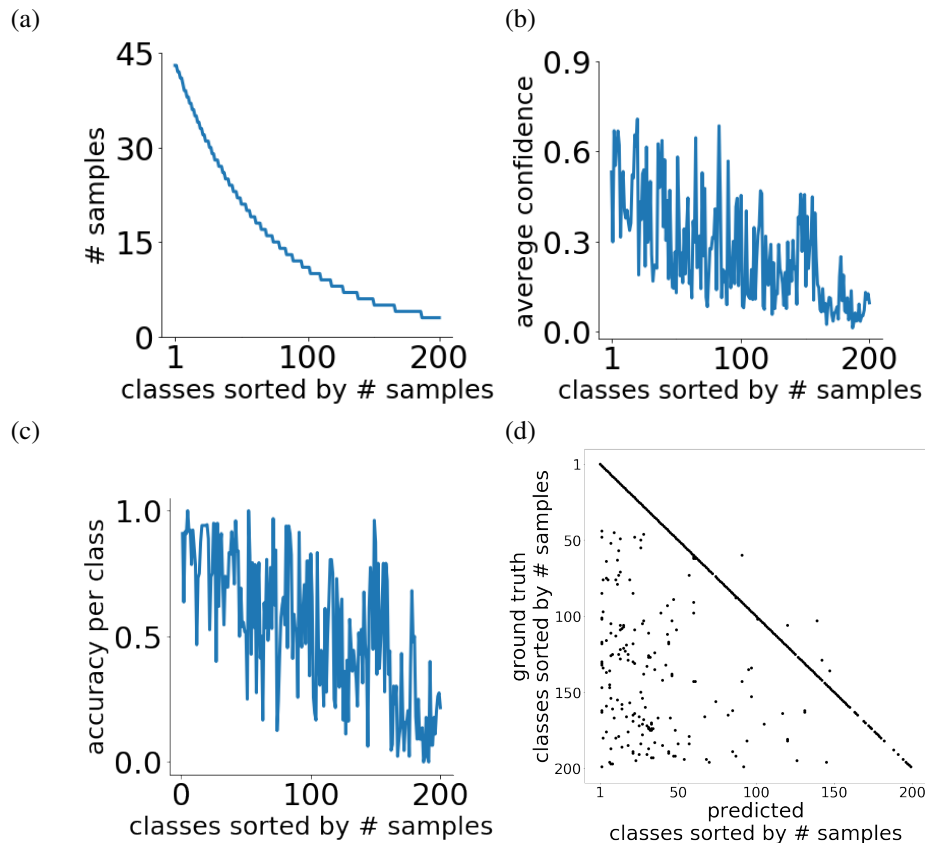


Figure 1: Unbalanced training data lead to a “familiarity bias”, where models output more confident and more accurate predictions for common classes compared with rare ones. **(a)** A long-tailed version of the CUB dataset [32]. Classes are ordered from left to right by their number of samples. **(b)** When training a ResNet-101 on long-tailed CUB, outputs tends to have low confidence for tail classes on the validation set. For each class, we show the mean output of the softmax for that class. **(c)** The classifier tends to have low accuracy for tail classes. **(d)** A confusion matrix of the classifier. The matrix shows markers for pairs of (gt, predicted) whose count is larger than 15.

the head classes; and an attribute classifier that is trained on per-class attributes and is expected to operate better on tail classes where the number of samples is small.

Our approach to address *data imbalance* is based on the following observation: Learning with unbalanced data leads to a **familiarity effect**, where models become biased to favor the more familiar, rich-sampled classes. Figure 1 illustrates this phenomenon. Panel 1(a) shows a long-tail variant of the CUB dataset [32], that was used for training a ResNet-101 to classify 200 bird species. Panel 1(b) shows the mean prediction score for each class, as measured on the validation set. Namely, for each class, we computed the output of softmax over *images from that class*. The model outputs more confident predictions when presented with common classes than rare ones. Panel 1(c) shows the accuracy for each class. The model is more accurate on head classes and makes more errors as the number of training samples decreases. Finally, Panel 1(d) provides the confusion matrix for this classifier, showing that the model mostly confuses low shot classes for head classes. Appendix A further analyzes the familiarity bias effect, showing that the approach described in this paper alleviates the effect. As an interesting side note, studies of human decision making and preference learning show a similar bias towards familiar classes. This effect is reported very widely and is related to the availability heuristic studied by Tversky and Kahneman [30].

Importantly, the familiarity effect caused by data imbalance has a crippling effect on aggregating predictions from multiple modalities. When per-modality predictions are consistently biased, it is difficult to combine information correctly from multiple modalities.

The current paper addresses the *data-imbalance* and the *data paucity* learning challenges, by addressing the familiarity effect in learning with attributes. We describe an easy-to-implement debiasing module that offsets the familiarity effect during training. It further learns to balance information from visual and text modalities. This module has a small number of parameters and is trained end-to-end jointly with the model. Interestingly, it explicitly learns how the number of samples non-linearly contributes to the familiarity bias.

The paper has three main contributions

1. The first model (DRAGON) addressing long-tail learning with attributes. (a) The model learns to offset the familiarity bias of unbalanced data. (b) This debiasing allows us to merge information from textual and visual data effectively.
2. A new benchmark split for evaluating long-tail learning with attributes for CUB, AWA and SUN image datasets. DRAGON outperforms all approaches designed for uni-modal long-tail learning on these benchmarks.
3. *New state-of-the-art (SoTA) results* for (a) learning with attributes on data with two-level distribution. (b) Long-tail learning (no attributes) on CIFAR-10 and CIFAR 100.

2 Related methods

Long-tail-learning: Long-tailed datasets usually cause models to favor the head of the distribution [5]. Previous efforts to address this effect typically take one of two approaches : Algorithmic approaches and data-manipulations approaches.

Algorithmic approaches include methods that force models to adjust their predictions to focus on training samples from poor classes, using a non-uniform cost per misclassification function. A natural approach is to re-scale the loss to penalize stronger errors for rare classes [11]. [17] proposed to down-weight the loss assigned to well-classified examples, preventing easy negatives from dominating the loss. Recently, [6] proposed a loss that encourages larger margins for rare classes, forcing a classifier to learn minority classes as well as majority classes. Finally, [12] observed that norm weights of a dot-product classifier trained on unbalanced data are correlated with class cardinality. To offset the bias, they L_2 -normalized the weights of each classifier. The correlation between the norm weights and class cardinality is related to the “familiarity effect” we describe. Yet, instead of observing it on static weights, we observe that it is applied dynamically to sample-based prediction scores.

Data-manipulation approaches aim to flatten long-tail datasets to correct the bias towards majority classes. Popular techniques employ over-sampling of minority classes, under-sampling the majority classes or generating samples from the minority classes. Overfitting the tail classes is the major drawback of oversampling minority classes, while discarding a lot of data samples is the main disadvantage of undersampling head classes. [4] shows that synthetic data can considerably reduce error rates for classes that are rare.

Another approach is to transfer meta-level-knowledge from data-rich classes to data-poor classes. [34] applied this idea and gradually transfer hyperparameters from rich classes to poor classes by representing knowledge as trajectories in model space that capture the evolution of parameters with increasing training samples.

Learning with attributes: Learning with attributes is usually applied to zero-shot learning (ZSL) [37, 16, 3], where a classifier is trained to recognize (new) unseen classes based on their semantic description, which can include a natural-language textual description or predefined attributes. In several ZSL studies, the attributes detected in a test image are matched with ground-truth attributes of each class, and several studies focused on this matching [16, 3, 28, 41, 40, 7]. For our attribute expert module, we use *LAGO* [3], a state-of-the-art approach for learning with attributes, which learns to combine attribute that describes classes using an AND-OR group structure.

A series of papers proposed to learn a shared representation of visual and text features (attributes). As one example, [29] learns such a shared latent manifold using autoencoders and then minimizes the MMD loss between the two domains. Another recent line of work synthesizes feature vectors of unseen classes using generative models like VAE or GAN, and then use them in training a

conventional classifier [21, 36, 10, 1, 20, 42, 26, 38]. The major baseline we compare our approach with is CADA-VAE [26], the current SoTA for Generalized FSL (GFSL) with attributes. CADA-VAE uses a variational autoencoder that aligns the distributions of image features and semantic (attribute) class embedding in a shared latent space.

Generalized ZSL (GZSL) and Generalized FSL (GFSL): GZSL extends ZSL to the scenario where the test data contains both seen and unseen classes [8, 37, 27]. Recently, GZSL was extended to Generalized Few-Shot-Learning with attributes (GFSL-a), where the unseen classes are augmented with a fixed number of few training samples [26, 29]. Namely, the distribution of samples across classes is a 2-level distribution, with many “head” classes having large number of samples, and a smaller set of “tail” classes all having the same (small) number of samples per class. Both GZSL and GFSL-a can be viewed as special cases of long-tail learning with attributes, but with a distribution that is not natural. Unlike common distribution over classes which decays smoothly, in these cases, the distribution over classes is a hard 2-level step function.

Among GZSL approaches, [2, 27, 39] are most related to the current paper. They use a gating mechanism to weigh the decisions of two experts, one for seen classes and another for unseen classes. The gating module is modeled as an out-of-distribution estimator. The current paper differs from their work in several ways. First, the problem setup is different. Here, all samples are *in-distribution* and rather than a two-level step function, the distribution of classes is smooth and long-tail with a much smaller number of head classes. Second, the architecture of the current model is designed to quantify and correct for the (smooth) familiarity effect, where the model outputs stronger and more confident predictions when presented with common classes than rare ones. The fusion-module adjusts the outputs of both expert for this effect and then learns how to fuse the debiased decision of the two experts.

A recent GFSL-a generative approach is [38], which is a mixture of VAEs and GANs using an unconditional discriminator. We could not directly compare with that method because their FSL protocol deviates from the standard benchmark of [37, 26] since the authors fine-tune the CNN features for the task. Note that, *without* fine-tuning, on the generalized zero-shot benchmark, their reported metrics are similar to [26] the main VAE benchmark that we compared within this paper.

Early vs late fusion: When learning from multiple modalities, one often distinguishes between early and late fusion models [18]. Early fusion models combine features from multiple modalities to form a joint representation. Late fusion methods combine decisions of per-modality models.

3 Long-tail learning with attributes

We provide a formal definition of long-tail learning with attributes.

A training set \mathcal{X}, \mathcal{Y} has n labeled image samples: $\mathcal{X}, \mathcal{Y} = \{(\mathbf{x}_i, y_i), i = 1 \dots n\}$, where each \mathbf{x}_i is a feature vector and $y_i \in \mathcal{Y}$ is a label from $\mathcal{Y} = \{1, 2, \dots k\}$. The samples are drawn from a distribution \mathcal{D} such that the marginal distribution over the classes $p(y)$ is strongly non uniform. For example, $p(y)$ may be exponential $p(y) \sim \exp(-ky)$.

As a second supervision signal, each class y is also accompanied with a *class-description* vector \mathbf{a}_y in the form of semantic attributes [16] or natural-language embedding [24, 42, 27]. For example, in the CUB dataset [32], a class may be annotated by attributes like `Head-color:red`.

At test time, a new set of samples $\mathcal{X}' = \{\mathbf{x}_i, i = n + 1, \dots, n + m\}$ is given from the same distribution \mathcal{D} . Our goal is to predict the correct class of each test sample.

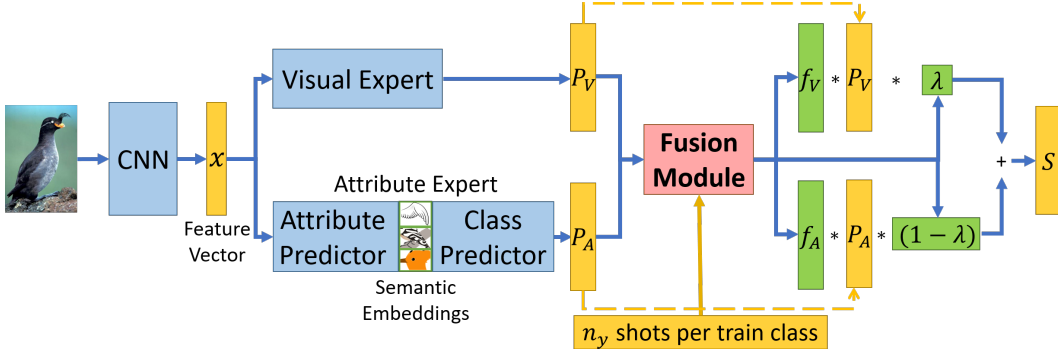


Figure 2: The DRAGON architecture for long-tail learning with attributes. In blue, network components. In yellow, input to the fusion module. In green, the outputs of the fusion module.

4 Our approach

We aim to address the key challenge of long-tail learning from multiple modalities: training a single model to perform well for both head classes and tail classes while fusing information from vision and language.

Our approach is based on two observations: (1) Attribute-based models provide relatively accurate predictions in the low-shot regime. This is because a class can be recognized by its attributes even with few or no training samples available [16, 37, 3] (and Appendix B). (2) The average prediction confidence for samples of a given class is correlated with the number of training samples for that class (Figure 1).

We design an architecture that leverages these observations by learning to adaptively (1) Combine predictions of two experts classifiers: A conventional visual expert which is more accurate for head classes and an attribute expert which excels at the tail classes; (2) Reweight the scores of each class prediction, based on the number of training samples for that class.

This approach can be viewed as achieving two tasks: It learns (1) to debias the predictions of each model; and (2) to combine the predictions of the two experts.

4.1 The architecture

We now describe DRAGON¹, an architecture for multi-modal long-tail learning. The architecture follows two design considerations: We want the model to be modular and to be light. First, modularity allows to plug-in and fuse multi-modal experts, each trained for its own modality. Here we use a language-based (attribute) expert and a visual expert, but we could consider any modality expert like mesh, depth, motion or multi-spectral information. Second, limiting the model to have a small number of parameters is important because tail classes only have few training samples and the model must perform well at the tail.

Our general architecture (Figure 2) takes a late fusion approach. The architecture consists of two experts modules: A visual expert, which is an image classifier that is trained in a standard way, and an attribute expert that predicts a class based on a semantic embedding of an image. Each expert outputs a prediction vector which is fed to a fusion-module. The fusion-module takes the experts predictions and learns to debias the familiarity effect, by weighing the experts and rescaling their class predictions.

More formally, given an input image, the architecture evaluates the following score per class y :

$$S(y) = \lambda f_V(y) p_V(y) + (1 - \lambda) f_A(y) p_A(y). \quad (1)$$

Here, $p_V(y)$ and $p_A(y)$ are raw confidence scores of a visual expert and the attribute expert; $f_V(y)$ and $f_A(y)$ are positive coefficients that re-scale the raw confidence scores of the experts to compensate

¹Dragons, like many distributions, have long tails and are cool. For acronym lovers, DRAGON also stands for “a moDular Approach for lonG-tail classificatiON”.

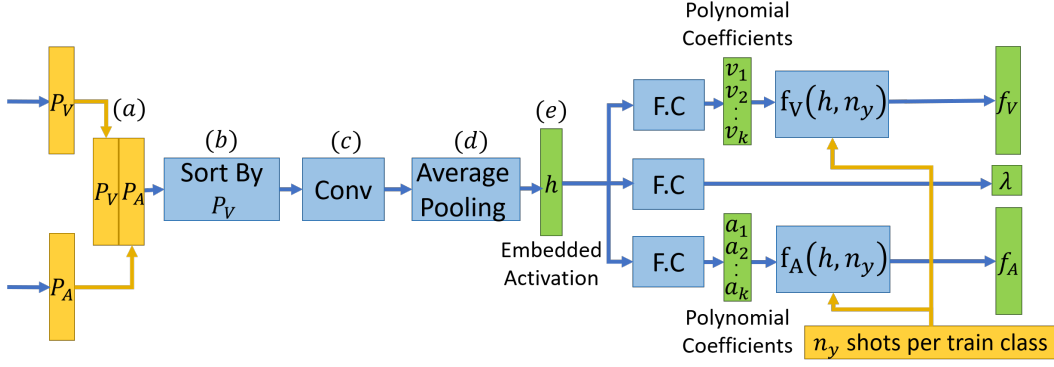


Figure 3: Architecture of the fusion-module for long-tail learning with attributes. In blue, network components. In yellow, inputs to the fusion-module and in green, activations or outputs of the fusion-module. The inputs P_V denote the softmax prediction vector of the *Visual Expert*, and P_A that of the *Attribute Expert*. The outputs f_V , f_A and λ are used in Eq. (1) for re-weighting the inputs. See Section 4.2 for more details.

for the familiarity effect; and $\lambda \in (0, 1)$, is a combination coefficient that balances the experts. It learns to exploit the familiarity effect (Figure 1) in order to account the more relevant expert.

Next, we describe the architecture of the fusion-module and its training setup.

4.2 A fusion-module

Given an image sample, the fusion-module outputs three components f_V , f_A and λ . $f_V(y)$ is a set of coefficients that reweigh each y class prediction scores for the visual expert and $f_A(y)$ is the same for the attribute expert. The two re-weighted expert predictions are combined with a coefficient λ . We leverage the observation that prediction confidence of a class is correlated with its number of training samples (Figure 1) and use the softmax output vectors of the two experts as the input of the fusion-module.

Figure 3 describes the architecture of the fusion-module. It has two main parts. The first part maps the prediction scores to a meaningful embedded space, in three steps. (a) Stack together the predictions of two experts to a $\mathcal{Y} \times 2$ vector. This makes the convolution meaningful across the 2 experts axis. (b) To make it also meaningful along the classes axis, and since classes are categorical, we reorder the classes, by their prediction score according to one of the experts. This sorts the predictions in a meaningful order, and couples together classes that are visually similar that the classifiers tend to confuse. (c) Coupling similar classes allows us to feed the sorted scores to a $N_{filters} \times 2 \times 2$ convolutional network. (d) The convolutional network is followed by an average pooling layer yielding a $(\mathcal{Y} - 1) \times 1$ embedding tensor. (e) We denote the by h the embedding function described above, and by \mathbf{h} its embedded activation: $\mathbf{h} = h(\mathbf{p}_V, \mathbf{p}_A)$, where \mathbf{p}_V , \mathbf{p}_A are vector notations for the prediction scores of each expert.

We now describe the second part, which takes \mathbf{h} and produces three outputs:

$$\begin{aligned}
 \lambda &= f_0(\mathbf{h}) \\
 f_V(y) &= [\mathbf{f}_V(\mathbf{h})](y) \\
 f_A(y) &= [\mathbf{f}_A(\mathbf{h})](y),
 \end{aligned} \tag{2}$$

where f_0 is a scalar output of a fully connected layer with a sigmoid activation, and $\mathbf{f}_V(\mathbf{h})$, $\mathbf{f}_A(\mathbf{h})$ are vector outputs that are used to re-scale the experts predictions according to Eq. (1). The key idea is very simple: We learn to reverse the familiarity effect, by fitting a function from the number of samples that a class has, to a debiasing weight over the confidence for that class.

Formally, $f_V(\mathbf{h})$ uses a fully connected layer to map the embedding vector \mathbf{h} to a $k \times 1$ polynomial coefficients \mathbf{v} that weights a class according to the number of its training samples. Similarly, $f_A(\mathbf{h})$ maps \mathbf{h} to a $k \times 1$ polynomial coefficients \mathbf{a} :

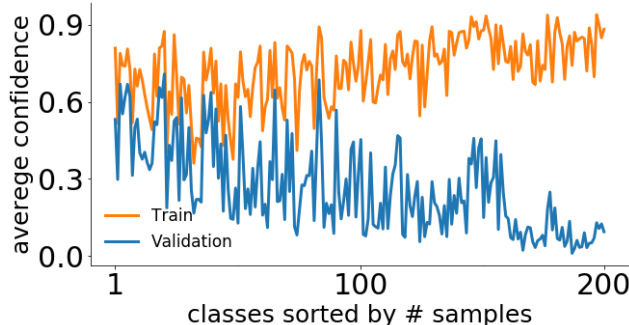


Figure 4: Train-validation mismatch of the familiarity effect: For *training* samples (orange), a classifier tends to produce highly confident scores for the tail classes. However, for *validation* samples (blue), the classifier produces low confidence scores for those classes (validation curve resembles Figure 1b). Predictions were generated by a ResNet101 trained on long-tailed CUB. We plot the mean confidence (softmax output) over all samples for each class.

$$\mathbf{f}_V(\mathbf{h}, n_y) = \sigma \left[\sum_{i=0}^{k-1} v_i \left(\frac{n_y}{\max_y(n_y)} \right)^i \right] \quad (3)$$

$$\mathbf{f}_A(\mathbf{h}, n_y) = \sigma \left[\sum_{i=0}^{k-1} a_i \left(\frac{n_y}{\max_y(n_y)} \right)^i \right] \quad (4)$$

where n_y is the number of training samples for a class y , k is the polynomial degree and σ denotes a sigmoid that ensures that the resulting scale is positive and non-zero. In Section 9 we study the contribution of each component of the approach with an ablation study and in Appendix C we give more intuition about the fusion module.

4.3 Training the fusion-module

Our goal is to have the fusion-module learn to capture the correlations between the number of training samples and the output confidence (the familiarity bias), so it can adjust for it.

Unfortunately, while the familiarity effect is substantial in the validation data and in the test data, it is not present in the training data. The reason is: Models tend to overfit and become overconfident over rare classes in the training set. This effect is illustrated in Figure 4 (compare Train versus Validation curves). To address this mismatch, we hold-out a subset of the training data and use it to simulate the response of experts to test samples. This set is used for training the fusion-module. We train the architecture with a cross-entropy loss over the outputs of $S(y)$ (Eq. (1)) L_1 normalized by their sum across classes, forcing a unit sum of class predictions.

5 Implementation details

Training: We train the architecture in three steps: First, we train each expert on the training data excluding the hold-out set. Second, we freeze the experts’ weights and train the *fusion-module* on all the training set. Finally, we re-train the experts on all the training data. For inference, we use the fusion-module trained at the second step with the experts trained at the third step.

Hyperparameter tuning: We chose the model that maximizes Acc_{WGT} on the validation set.

Platt-scaling: We use Platt-scaling [23] to tune the combination coefficient λ by adding constant bias β and applying a sigmoid on top of its scores: $\lambda = \sigma[f_0 - \beta]$, where β is a hyper parameter selected with cross validation.

Visual expert: We trained a logistic regression classifier over pretrained ResNet features to predict $p(y|\mathbf{x})$. We used a cross-entropy loss, weighted by class distribution and L_2 regularization.

Attribute expert: For the attribute expert we use LAGO [3], with a weighted cross-entropy loss. We used the implementation and hyper parameters provided by the authors.

Fusion-module: We trained the fusion-module with Adam [14] optimizer. Learning rate, and the polynomial degree were chosen by hyper parameter optimization.

6 Experimental setup overview

We evaluate DRAGON in two unbalanced benchmark scenarios. First, “*Smooth-Tail*”, a long-tail setup where the distribution of classes smoothly decays exponentially (Figure 5). Second, “*Two-Level*”, a two-level distribution, as in [26], where a large fraction of classes have many samples, and the rest have few samples (Figure 6). We compared it to 4 SoTA approaches, 5 natural and strong baselines and 6 other ablated architectures.

The experimental framework is based on [26] and [37, 35], which is the common experimental framework for comparing GZSL methods. Our evaluation uses their features (ResNet-101 [13]), and where applicable, also uses their cross-validation splits and evaluation metrics to allow direct comparisons with the SoTA baselines.

Datasets: We evaluate DRAGON on 3 widely-used datasets for learning with attributes.

1. *CUB-200-2011* [32] contains 11,788 visual images of 200 bird species for fine-grained classification. Each species is described by 312 binary attributes (like tail-pattern:solid, wing-color:black).
2. *SUN* [22], contains 14,340 complex visual scenes, from 717 scene types and 102 attributes (like material:rock, function:eating, surface:glossy).
3. *AWA* [16], consists of 30,475 images of 50 animal classes and 85 attributes (like texture:furry, or color:black).

Hold-out set: For the hold-out set, we randomly draw 50% of the samples of the tail classes and 20% of the samples of the head classes. For the long-tail split, we aligned with the 2-step split in [37, 26] to select whether to draw 50% or 20% of its samples. See Appendix D.3 for details.

Hyper-parameter tuning: We selected hyper parameters and evaluated different architecture alternatives on a validation set. We optimized the following hyper-parameters: (1) Number of filters in the convolution layer $\in \{1, \dots, 4\}$. (2) Degree of polynomial in Eq.4 $\in \{2, 3, 4\}$. (3) Learning rate $\in \{10^{-5}, 10^{-4}, 10^{-3}\}$ (4) Platt bias term $\beta \in [-2, 2]$.

6.1 Baselines and variants

We compared DRAGON with SoTA approaches and with other baselines:

1. *Most Common Class:* Predicting the common class for every test sample.
2. *Cross Entropy:* A model trained with a cross-entropy loss.
3. *Up-sampling All Classes* and training a model with cross-entropy loss.
4. *Visual Expert:* An object recognition classifier trained using weighted cross-entropy loss and L_2 regularization (Sec. 5).
5. *Attribute Expert:* LAGO [3], a SoTA ZSL model trained with a weighted cross-entropy loss.
6. *Anchor* [25]: A SoTA long-tail learning approach that penalizes the network to avoid the score of a false prediction being significant, by dynamically rescaling the cross-entropy loss based on the prediction difficulty of a sample.
7. *LDAM* [6]: A SoTA long-tail learning approach that encourages larger margins for rare classes.
8. *ReViSE* [29]: Learns a shared latent manifold between image features and class attributes using autoencoders. It then minimizes the maximum mean discrepancy (MMD) loss between the two domains.
9. *CA-VAE* and *DA-VAE* are two forms of latent distribution matching and reconstruction techniques for a VAEs as proposed by [26]. CA and DA refers to training with Cross-Alignment Loss and Distribution-Alignment Loss.

10. *CADA-VAE* [26]: The current SoTA for GFSL with attributes. A *generative approach* that uses a variational auto encoder with a shared latent space of image features and semantic (attribute) class embeddings. It uses a combination of CA Loss and DA Loss for reconstruction. For training CADA-VAE on the Smooth-Tail benchmark, we followed [26] protocol as closely as we could. See Appendix D for details.

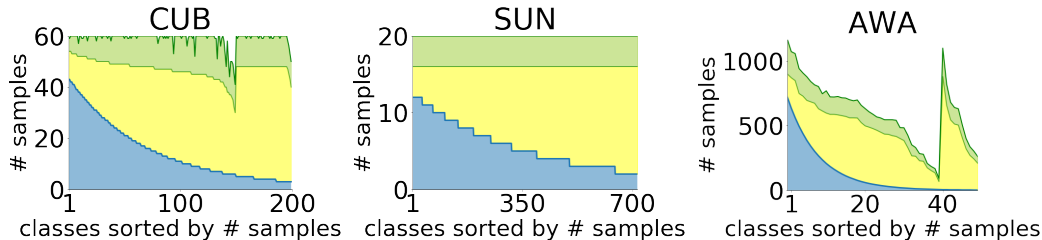


Figure 5: Long-tailed versions of CUB, SUN and AWA. Training sets are shown in blue. They were created by applying an exponential function of the form $(a * b^{-x})$ to the original training set of each dataset. In yellow, samples assigned to the pool of potential validation samples. In green, same for the test set. For evaluations, we weigh per-class accuracy such that the validation and the test distribution match the long-tail training attribution.

7 Smooth-Tail benchmark

To evaluate DRAGON in a long-tail learning scenario we created new variants with long-tail distribution of the three main learning-with-attributes benchmarks - CUB, SUN and AWA. Figure 5 illustrates these distributions. The long-tail distribution was created by ranking the classes based on the number of samples while making sure that the classes at its tail overlap with the tail classes of Two-Level as described later in Section 8. To select how many samples to draw, we applied an exponential function of the form ab^{-rank} . Here, a and b were selected such that the first class has the maximum number of samples, and the last class has 2 or 3 samples depending on the dataset. This allows us to ensure that tail classes have a small number of samples as desired. The exponential function decides how many samples each class contains, those samples are chosen randomly, and the remain samples are assigned to the validation set. Appendix D, describes the long-tail splits for CUB, SUN and AWA in more details.

7.1 Evaluation metrics

We evaluated the Smooth-Tail benchmark with the following metrics:

1. *Per-Class Accuracy* (Acc_{PC}): Balanced accuracy metric that uniformly averages the individual accuracy of each class $\frac{1}{k} \sum_{y=1}^k Acc(y)$, where $Acc(y)$ is the accuracy of class y and k is the number of classes.
2. *Weighted Accuracy* (Acc_{WGT}): Test accuracy, where the distribution over test classes is long-tailed like the training distribution. This is expected to be the typical case in real-world scenarios.

In practice, the number of samples available for testing in many datasets does not adhere to the train distribution. To compute this metric we therefore computed the accuracy of each class $Acc(y)$, and then computed their weighted average based on the train distribution over classes $\sum_{y=1}^k p_{train}(y)acc(y)$, where $0 < p_{train}(y) < 1$, $\sum_y p_{train}(y) = 1$ ². This is equivalent to transforming the test set to have the same distribution as the train set.

7.2 Results with smooth-tail distribution

Table 1 provides the test accuracy for the three long-tail benchmark datasets and compare DRAGON to baselines and to individual components of the DRAGON model. DRAGON achieves higher accuracy

²An early submission of this work calculated this metric using bootstrap. The results of that calculation were incorrect due to a Tensorflow issue with random-number generation.

| LONG-TAIL | CUB | | SUN | | AWA | |
|-----------------------------|-------------|-------------|-------------|-------------|-------------|-------------|
| | Acc_{PC} | Acc_{WGT} | Acc_{PC} | Acc_{WGT} | Acc_{PC} | Acc_{WGT} |
| BASELINES | | | | | | |
| MOST COMMON CLASS | 0.50 | 1.40 | 0.14 | 0.20 | 2.00 | 11.6 |
| CROSS ENTROPY | 47.6 | 65.0 | 27.4 | 35.4 | 61.5 | 92.8 |
| ANCHOR [25] | 48.3 | 64.7 | 28.2 | 36.2 | 59.1 | 93.2 |
| LDAM [6] | 50.1 | 64.1 | 29.8 | 36.4 | 69.1 | 93.5 |
| UP-SAMPLING ALL CLASSES | 50.0 | 65.1 | 29.1 | 36.4 | 68.5 | 93.4 |
| CADA-VAE [26] | 48.3 | 57.4 | 32.8 | 35.1 | 73.5 | 89.5 |
| DRAGON & MODULES | | | | | | |
| VISUAL EXPERT | 53.0 | 65.5 | 33.7 | 40.0 | 73.7 | 93.4 |
| ATTRIBUTE EXPERT | 54.8 | 66.0 | 18.2 | 18.3 | 74.0 | 93.0 |
| DRAGON (OURS) | 57.8 | 67.7 | 34.8 | 40.4 | 74.0 | 94.0 |

Table 1: Comparing DRAGON with baselines on the long-tailed benchmark datasets. We report Per-Class Accuracy Acc_{PC} and Weighted Accuracy Acc_{WGT} .

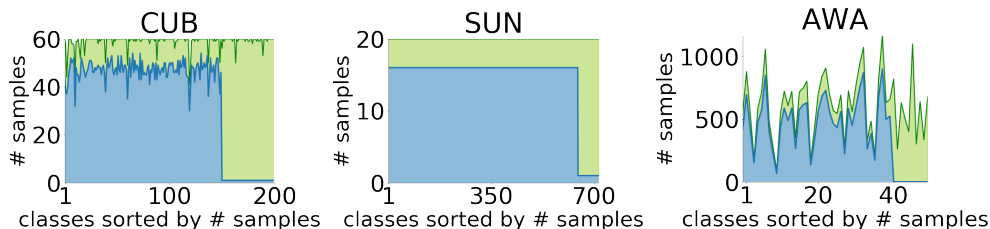


Figure 6: Two-level variants of the CUB, SUN and AWA benchmarks as proposed in [26]. Blue areas denote samples allocated to the training set, and green areas for samples allocated to the test set. For evaluations, we weigh per-class accuracy such that the validation distribution and the test distribution match the training attribution.

compared with all competing methods, both with respect to class-balanced accuracy (Acc_{PC}) and to test-distribution accuracy (Acc_{WGT}). The accuracy improvements of Acc_{PC} is largest for CUB, where it improves from 50.1% to 57.8%, a relative gain of 15.4%. The increase in Acc_{WGT} is largest for SUN, where it improves from 36.4% to 40.4%, a relative gain of 11.0%.

Improving Acc_{WGT} indicates that DRAGON effectively classifies head classes, which are heavily weighted in Acc_{WGT} . At the same time, improving Acc_{PC} indicates that DRAGON also effectively classifies tail classes, which are up-weighted in Acc_{PC} .

The total training time of our proposed solution is approximately 3 minutes, on a single NVIDIA Tesla K40m GPU.

8 Two-Level benchmark

The Two-Level benchmark (Figure 6) follows the protocol of [26]. For all datasets, many-shot classes have remained the same as in the train-set while few-shot classes have increasing number of shots: 1,2,5,10 and 20 (in SUN up to 10 shots).

8.1 Evaluation metrics

We evaluated the Two-Level benchmark with standard metrics from [26]:

1. *Many-Shot Accuracy* (Acc_{MS}): Per-class accuracy over many-shot classes. The model is only evaluated on the samples which are labeled as rich classes, and reported as Acc_{MS} .
2. *Few-Shot Accuracy* (Acc_{FS}): Per-class accuracy over few-shot classes. The model is only evaluated on the samples which are labeled as poor classes, and reported as Acc_{FS} .

3. *Harmonic Accuracy* (Acc_H): Harmonic mean of Acc_{MS} and Acc_{FS} . $Acc_H = 2(Acc_{MS}Acc_{FS})/(Acc_{MS} + Acc_{FS})$. This metric shows us the balance between model’s strength on head classes and tail-classes.

8.2 Results with two-level distribution

Table 2 compares DRAGON with SoTA baselines on the two-level splits. Our model gives the same or better results compared to baselines although DRAGON is much simpler to train and tune. It wins in CUB and SUN on all shots but loses on AWA when fewer than 10 samples are available. Furthermore, DRAGON excels when the number of shots increases in contrast to complex generative models. Appendix E.1 provides results for Acc_{FS} and Acc_{MS} .

| # SHOTS | CUB | | | | | SUN | | | | AWA | | | | |
|----------------------|-------------|-------------|-------------|-------------|-------------|-------------|-------------|-------------|-------------|-------------|-------------|-------------|-------------|-------------|
| | 1 | 2 | 5 | 10 | 20 | 1 | 2 | 5 | 10 | 1 | 2 | 5 | 10 | 20 |
| MOST COMMON CLASS | 0 | 0 | 0 | 0 | 0 | 0 | 0 | 0 | 0 | 0 | 0 | 0 | 0 | 0 |
| LDAM [6] | 2.4 | 10.9 | 36.0 | 52.2 | 61.5 | 4.3 | 11.5 | 26.6 | 37.0 | 12.4 | 24.8 | 41.1 | 57.0 | 68.6 |
| REVISE [29] | 36.3 | 41.1 | 44.6 | 50.9 | - | 27.4 | 33.4 | 37.4 | 40.8 | 56.1 | 60.3 | 64.1 | 67.8 | - |
| CA-VAE [26] | 50.6 | 54.4 | 59.6 | 62.2 | - | 37.8 | 41.4 | 44.2 | 45.8 | 64.0 | 71.3 | 76.6 | 79.0 | - |
| DA-VAE [26] | 49.2 | 54.6 | 58.8 | 60.8 | - | 37.8 | 40.8 | 43.6 | 45.1 | 68.0 | 73.0 | 75.6 | 76.8 | - |
| CADA-VAE [26] | 55.2 | 59.2 | 63.0 | 64.9 | 66.0 | 40.6 | 43.0 | 46.0 | 47.6 | 69.6 | 73.7 | 78.1 | 80.2 | 80.9 |
| VISUAL EXPERT | 1.2 | 6.9 | 30.2 | 50.2 | 60.9 | 1.8 | 8.9 | 25.1 | 38.3 | 11.0 | 20.0 | 47.8 | 69.9 | 73.9 |
| LAGO | 23.0 | 33.2 | 49.0 | 58.6 | 64.8 | 19.5 | 23.2 | 25.6 | 27.8 | 20.2 | 33.0 | 59.0 | 68.7 | 75.8 |
| DRAGON (OURS) | 55.3 | 59.2 | 63.5 | 67.8 | 69.9 | 41.0 | 43.8 | 46.7 | 48.2 | 67.1 | 69.1 | 76.7 | 81.9 | 83.3 |

Table 2: Comparing DRAGON with SoTA GFSL models and baselines with increasing number of few-shot training samples. Values denote the per-class Harmonic Accuracy.

9 Ablation study

To understand the contribution of the different modules of DRAGON, we carried ablation experiments and quantify the benefits of various components of the fusion-module architecture. We first compare different variants of the fusion-module, then evaluate the contribution of sorting the inputs to the module, and finally, show the difference in performance when training with or without a hold-out set.

Fusion-Module Architecture: Table 3 shows the performance of various components of the fusion-module of Smooth-Tail CUB. (1) *Simple Avg.* averages \mathbf{p}_V with \mathbf{p}_A across classes. (2) *F.C.* is a simple Fully-Connected layer over \mathbf{p}_V \mathbf{p}_A to produce f_0 , without rescaling (setting $f_V(y) = 1, f_A(y) = 1$). (3) *F.C. & $1/n_y$ re-scale* learns expert weights as in *F.C.* and re-scales both experts predictions by n_y , the number of training samples of each class. (4) *F.C. & non-parametric re-scale* learns expert weights as *F.C.* and re-scales both experts predictions by a learned non-parametric weight for each class. (5) *Conv. & non-parametric re-scale* is like (4), and applies the sorting and convolution as described in Section 4.2. (6) *Conv. & single parametric re-scale* replaces the non-parametric rescaling weights by a single polynomial of parametrized weights. (7) DRAGON is our full approach as described in section 4, using two polynomials of re-scaling parametrized weights.

First, we note that Acc_{PC} shows the most significant improvement, indicating the effectiveness of our approach on tail classes. Second, we find that all ablated components synergistically contribute to the quality metrics. The ablation results are consistent with ablation on the test set (Appendix E.2).

Sorting: Table 4 (Left) shows the importance of sorting base experts’ predictions as input to our fusion-module. (1) *No-Sorting* relates to using raw experts’ predictions without any processing. (2) *Sorting-By-Visual-Expert* relates to sorting both experts’ predictions together according to the values of the Visual Expert predictions (argsort). (3) *Sorting-By-Attribute-Expert* is the same as (2) but sorting experts’ predictions by values of Attribute Expert predictions.

Training Process: Table 4 (Right) describes the performance of the DRAGON architecture when trained naively without a hold-out set: (1) *All-Train:* Training the DRAGON fusion-module naively

| | Acc_{PC} | Acc_{WGT} |
|--|-------------|-------------|
| SIMPLE AVG. | 56.2 | 66.5 |
| F.C. | 56.5 | 66.2 |
| F.C. & $1/n_y$ RE-SCALE | 56.3 | 55.9 |
| F.C. & NON-PARAMETRIC RE-SCALE | 56.8 | 65.1 |
| CONV. & NON-PARAMETRIC RE-SCALE | 56.1 | 66.8 |
| CONV. & SINGLE PARAMETRIC RE-SCALE | 55.4 | 64.5 |
| DRAGON (OURS) (CONV & DUAL PARAMETRIC RE-SCALE) | 57.0 | 67.0 |

Table 3: Ablation study on Smooth-Tail CUB. The results show the contribution of the convolutional backbone and of rescaling the two experts using a parametric mapping. Reported values are computed over the validation set.

| SORTING | Acc_{PC} | Acc_{WGT} | TRAINING PROCESS | Acc_{PC} |
|-----------------------------|-------------|-------------|-----------------------------|-------------|
| NO-SORTING | 55.3 | 66.1 | ALL-TRAIN | 49.6 |
| SORTING-BY-VISUAL-EXPERT | 57.0 | 67.0 | END-TO-END | 42.3 |
| SORTING-BY-ATTRIBUTE-EXPERT | 56.8 | 66.9 | THREE-STAGE-TRAINING | 57.0 |

Table 4: Ablation study on the validation set of Smooth-Tail CUB. Results quantify the contribution of sorting the fusion-module inputs (left) and the effect of three-stage training (right).

without a hold-out set. (2) *End-To-End*: Training all the architecture (both experts and fusion-module) end to end. (3) *Three-Stage-Training*: Training our models as explained in section 5.

10 Extension to vision-only long-tail learning

The approach presented in this paper focuses on learning from two modalities: vision and language. A simpler variant of the model can be applied to learning with visual samples only. In this setting, the fusion-module only learns to offset the predictions of a visual model. We name it smDRAGON for *single-modality*-DRAGON, and show below that it achieves new state-of-the-art results on CIFAR-10 and CIFAR-100.

To adapt to single-modality, we train smDRAGON only on the predictions of a visual expert and use a simplified fusion-module. This module outputs a single set of coefficients $\{f_V(y)\}_{y \in \mathcal{Y}}$ to re-scale the predictions of the visual expert, instead of two sets of coefficients. Subsequently, Eq. 1 reduces to

$$S(y) = f_V(y)p_V(y) \quad . \quad (5)$$

We evaluated smDRAGON on long-tail CIFAR-10 and CIFAR-100 [15]. We tested two different distributions: long-tail and two-level, each with two different imbalance ratios $p = 100$ and $p = 10$, as proposed by [6].

Tables 5,6 compares smDRAGON with popular baselines and common techniques used to address unbalanced datasets [6]. They demonstrates that (1) DRAGON outperforms all baselines (2) When combining DRAGON with SoTA approaches (LDAM or DRW) it further improves their results.

Specifically, Table 5 shows that smDRAGON achieves new SoTA results in most scenarios just by using a ResNet-32, trained using a traditional cross-entropy loss as its backbone. It compares the error-rate (lower is better) for a set of baseline approaches as was reported by [6]. Rows with * denote results that were reproduced using code published by the authors of [6].

| DATASET | UNBALANCED CIFAR-10 | | | | UNBALANCED CIFAR-100 | | | |
|---------------------|---------------------|--------------|--------------|--------------|----------------------|--------------|--------------|--------------|
| | LONG-TAIL | | TWO-LEVEL | | LONG-TAIL | | TWO-LEVEL | |
| IMBALANCE RATIO | 100 | 10 | 100 | 10 | 100 | 10 | 100 | 10 |
| CB ReSAMPLE [9] | 29.45 | 13.21 | 38.14 | 15.41 | 66.56 | 44.94 | 66.23 | 46.92 |
| CB ReWEIGHT [9] | 27.63 | 13.46 | 38.06 | 16.20 | 66.01 | 42.88 | 78.69 | 47.52 |
| CB FOCAL [9] | 25.43 | 12.90 | 39.73 | 16.54 | 63.98 | 42.01 | 80.24 | 49.98 |
| CE [6] | 29.64 | 13.61 | 36.70 | 17.50 | 61.68 | 44.30 | 61.45 | 45.37 |
| CE* | 29.81 | 13.12 | 36.61 | 17.78 | 61.72 | 43.77 | 61.59 | 45.75 |
| FOCAL [17] | 29.62 | 13.34 | 36.09 | 16.36 | 61.59 | 44.22 | 61.43 | 46.54 |
| LDAM [26] | 26.65 | 13.04 | 33.42 | 15.00 | 60.40 | 43.09 | 60.42 | 43.73 |
| CE* SMDRAGON | 22.08 | 12.17 | 27.10 | 12.38 | 58.01 | 42.22 | 54.43 | 40.97 |

Table 5: Error rate of ResNet-32 on unbalanced CIFAR-10 and CIFAR-100, comparing smDRAGON and state-of-the-art techniques. smDRAGON was trained over predictions of the cross-entropy model. Reported values are the top-1 validation error. Asterisks * denote results reproduced using code published by the authors of [6].

| DATASET | UNBALANCED CIFAR-10 | | | | UNBALANCED CIFAR-100 | | | |
|---------------------------|---------------------|--------------|--------------|--------------|----------------------|--------------|--------------|--------------|
| | LONG-TAIL | | TWO-LEVEL | | LONG-TAIL | | TWO-LEVEL | |
| IMBALANCE RATIO | 100 | 10 | 100 | 10 | 100 | 10 | 100 | 10 |
| M-DRW [33] | 24.94 | 13.57 | 26.67 | 13.17 | 59.49 | 43.49 | 58.91 | 44.72 |
| LDAM-DRW [6] | 22.97 | 11.84 | 23.08 | 12.19 | 57.96 | 41.29 | 54.64 | 40.54 |
| LDAM-DRW* [6] | 22.96 | 11.84 | 23.41 | 12.20 | 57.89 | 41.61 | 54.65 | 43.48 |
| CE-DRW* | 24.73 | 13.52 | 28.65 | 13.90 | 59.23 | 42.19 | 58.93 | 45.00 |
| CE-DRW* SMDRAGON | 20.37 | 12.06 | 21.54 | 11.94 | 56.50 | 42.11 | 53.32 | 40.66 |
| LDAM-DRW* SMDRAGON | 21.22 | 11.84 | 20.64 | 12.37 | 56.70 | 41.32 | 54.07 | 40.35 |

Table 6: smDRAGON with DRW or LDAM [6]. This table is similar to Table 5 except that all models were trained with DRW schedule [6], and smDRAGON was also applied over the LDAM approach. Reported values are top-1 validation error. Asterisks * denote results that we reproduced using code published by the authors of [6].

We compare DRAGON with the following baselines.

1. *CE*: A standard cross entropy loss.
2. *CB Resample* [9]: The training set is re-sampled with a probability proportional to effective number of samples in each class i , defined as $(1 - \beta^{n_i}) / (1 - \beta)$, where $\beta = (N - 1) / N$ and N is the number of unique prototypes.
3. *CB Reweight* [9]: The loss of each sample is weighted by $(1 - \beta^{n_i}) / (1 - \beta)$ defined above.
4. *Focal Loss* [17]: Down-weight the loss assigned to well-represented samples. This prevents easy negatives from overwhelming the model during training.
5. *LDAM Loss* [6]: Current SoTA loss function for unbalanced datasets. It encourages larger margins for rare classes, hence forcing a model to accurately classify tail classes as well as head classes.

Table 6 shows the effect of combining smDRAGON with existing SoTA approaches, yielding further improvement. It compares DRAGON with the current state-of-the-art baselines. Where smDRAGON and baselines were trained with deferred re-balancing (DRW), an optimization schedule proposed by [6]. The accuracy of smDRAGON with DRW is better or equivalent to all DRW-based baselines.

11 Conclusion

This paper discussed two key challenges for learning with attributes of long-tail, unbalanced data: First, a “familiarity bias” effect occurs, where models favor head classes and it hampers fusing information from multiple sources. Second, the low count of samples of tail classes leads to overfitting and poor accuracy for those classes. To address these challenges, we proposed a late-fusion architecture called DRAGON, which is modular and has small number of trainable parameters. This approach has three components: a visual expert model which excels on head classes, a semantic attribute expert model which excels on tail classes and a fusion-module that debiases and combines those experts predictions. Our method achieves improvement on long-tailed versions of three popular benchmark datasets, CUB, SUN and AWA. It also sets new state-of-the-art performance on a Two-Level benchmarks, compared to recent proposed methods.

DRAGON was designed as a late-fusion modular architecture, that combines the prediction of experts. The advantage of this approach is that one can plug new expert when they are developed, and makes training simple. as one potential drawback, it is possible that sharing information between visual and semantic experts earlier, could have improved performance even further.

We also introduced a simpler variant of DRAGON, called smDRAGON, designed for learning with visual samples only without additional semantic information. smDRAGON achieves new state-of-the-art results on existing benchmarks unbalanced CIFAR-10 and CIFAR-100. These results suggest that information about the number of samples per-class can be effectively use to reduce prediction biases.

Strongly unbalanced data with long tail is ubiquitous in numerous domains and problems. The results in this paper show that some of the challenges introduced by class imbalance can be alleviated using simple trainable models

Acknowledgments

This study was funded by a grant to GC from the Israel Science Foundation (ISF 737/2018), and by an equipment grant to GC and Bar-ILan University from the Israel Science Foundation (ISF 2332/18).

References

- [1] Arora, G., Verma, V.K., Mishra, A., Rai, P.: Generalized zero-shot learning via synthesized examples. In: CVPR (2018)
- [2] Atzmon, Y., Chechik, G.: Adaptive confidence smoothing for generalized zero-shot learning. CVPR (2018)
- [3] Atzmon, Y., Chechik, G.: Probabilistic and-or attribute grouping for zero-shot learning. In: UAI (2018)
- [4] Beery, S., Liu, Y., Morris, D., Piavis, J., Kapoor, A., Meister, M., Perona, P.: Synthetic examples improve generalization for rare classes. Preprint arXiv:1904.05916 (2019)
- [5] Buda, M., Maki, A., Mazurowski, M.A.: A systematic study of the class imbalance problem in convolutional neural networks. Neural Networks (2018)
- [6] Cao, K., Wei, C., Gaidon, A., Arechiga, N., Ma, T.: Learning imbalanced datasets with label-distribution-aware margin loss. Advances in Neural Information Processing Systems (2019)
- [7] Changpinyo, S., Chao, W.L., Gong, B., Sha, F.: Synthesized classifiers for zero-shot learning. In: CVPR (2016)
- [8] Chao, R., Changpinyo, S., Gong, B., F., S.: An empirical study and analysis of generalized zero-shot learning for object recognition in the wild. In: ICCV (2016)
- [9] Cui, Y., Jia, M., Lin, T.Y., Song, Y., Belongie, S.J.: Class-balanced loss based on effective number of samples. 2019 IEEE/CVF Conference on Computer Vision and Pattern Recognition (CVPR) pp. 9260–9269 (2019)
- [10] Felix, R., Kumar, V., Reid, I., Carneiro, G.: Multi-modal cycle-consistent generalized zero-shot learning. In: ECCV (2018)
- [11] He, H., Garcia, E.A.: Learning from imbalanced data. IEEE Transactions on Knowledge and Data Engineering (2009)
- [12] Kang, B., Xie, S., Rohrbach, M., Yan, Z., Gordo, A., Feng, J., Kalantidis, Y.: Decoupling representation and classifier for long-tailed recognition. ICLR (2020)
- [13] K.He, Zhang, X., Ren, S., Sun, J.: Deep residual learning for image recognition. In: CVPR (2016)
- [14] Kingma, D.P., Ba, J.: Adam: A Method for Stochastic Optimization. ICLR (2015)
- [15] Krizhevsky, A.: Learning multiple layers of features from tiny images (2009)
- [16] Lampert, C., Nickisch, H., Harmeling, S.: Learning to detect unseen object classes by between-class attribute transfer. In: CVPR (2009)
- [17] Lin, T.Y., Goyal, P., Girshick, R.B., He, K., Dollár, P.: Focal loss for dense object detection. ICCV (2017)
- [18] Liu, K., Li, Y., Xu, N., Natarajan, P.: Learn to combine modalities in multimodal deep learning. arXiv preprint arXiv:1805.11730 (2018)
- [19] Liu, Z., Miao, Z., Zhan, X., Wang, J., Gong, B., Yu, S.X.: Large-scale long-tailed recognition in an open world. In: CVPR (2019)
- [20] Mishra, A., Reddy, M., Mittal, A., Murthy, H.A.: A generative model for zero shot learning using conditional variational autoencoders. In: WACV (2018)
- [21] Pambala, A., Dutta, T., Biswas, S.: Generative model with semantic embedding and integrated classifier for generalized zero-shot learning. In: WACV (2020)
- [22] Patterson, G., Hays, J.: Sun attribute database: Discovering, annotating, and recognizing scene attributes. In: CVPR (2012)
- [23] Platt, J.C.: Probabilistic outputs for support vector machines and comparisons to regularized likelihood methods. In: Advances in large margin classifiers (1999)
- [24] Reed, S., Akata, Z., Lee, H., Schiele, B.: Learning deep representations of fine-grained visual descriptions. In: CVPR (2016)
- [25] Ryoo, S., Jeong, S.G., Perona, P.: Anchor loss: Modulating loss scale based on prediction difficulty. In: ICCV (2019)

- [26] Schönfeld, E., Ebrahimi, S., Sinha, S., Darrell, T., Akata, Z.: Generalized zero-shot learning via aligned variational autoencoders. In: CVPR (2019)
- [27] Socher, R., Ganjoo, M., Manning, C., Ng, A.: Zero-shot learning through cross-modal transfer. In: NIPS (2013)
- [28] Sung, F., Yang, Y., Zhang, L., Xiang, T., Torr, P.H., Hospedales, T.M.: Learning to compare: Relation network for few-shot learning. In: CVPR (2018)
- [29] Tsai, Y.H., Huang, L.K., Salakhutdinov, R.: Learning robust visual-semantic embeddings. In: ICCV (2017)
- [30] Tversky, A., Kahneman, D.: Availability: A heuristic for judging frequency and probability. *Cognitive psychology* (1973)
- [31] Van Horn, G., Perona, P.: The devil is in the tails: Fine-grained classification in the wild. arXiv preprint arXiv:1709.01450 (2017)
- [32] Wah, C., Branson, S., Welinder, P., Perona, P., Belongie, S.: The Caltech-UCSD Birds-200-2011 Dataset. Tech. Rep. CNS-TR-2011-001, California Institute of Technology (2011)
- [33] Wang, F., Cheng, J., Liu, W., Liu, H.: Additive margin softmax for face verification. *IEEE Signal Processing Letters* (2018)
- [34] Wang, Y.X., Ramanan, D., Hebert, M.: Learning to model the tail. In: NIPS (2017)
- [35] Xian, Y., Lampert, C., Schiele, B., Akata, Z.: Zero-shot learning - A comprehensive evaluation of the good, the bad and the ugly. TPAMI (2018)
- [36] Xian, Y., Lorenz, T., Schiele, B., Akata, Z.: Feature generating networks for zero-shot learning. In: CVPR (2018)
- [37] Xian, Y., Schiele, B., Akata, Z.: Zero-shot learning - the good, the bad and the ugly. In: CVPR (2017)
- [38] Xian, Y., Sharma, S., Schiele, B., Akata, Z.: F-vaegan-d2: A feature generating framework for any-shot learning. CVPR (2019)
- [39] Zhang, H., Koniusz, P.: Model selection for generalized zero-shot learning. In: ECCV (2018)
- [40] Zhang, H., Koniusz, P.: Zero-shot kernel learning. In: CVPR (2018)
- [41] Zhang, L., Xiang, T., Gong, S.: Learning a deep embedding model for zero-shot learning. In: CVPR (2017)
- [42] Zhu, Y., Elhoseiny, M., Liu, B., Peng, X., Elgammal, A.: A generative adversarial approach for zero-shot learning from noisy texts. In: CVPR (2018)

A Additional Analysis of the Familiarity Bias Effect

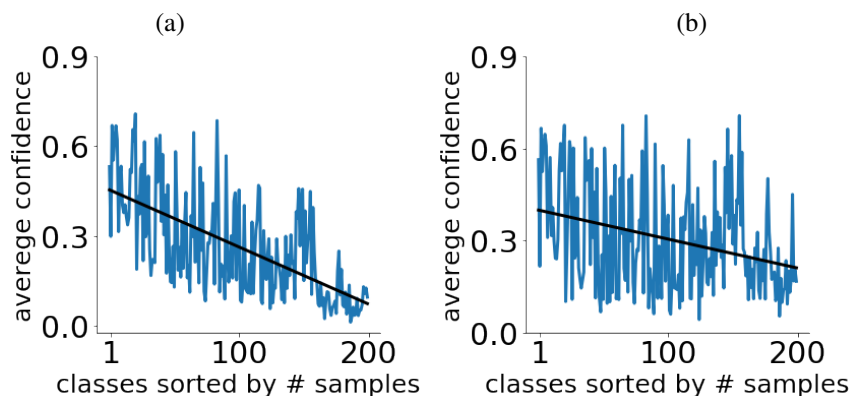


Fig. S 7: DRAGON learns to offset the familiarity bias. **(a)** Average-confidence per-class of a ResNet101 trained on long-tailed CUB as a function of the number of samples per class. **(b)** Similar curve for DRAGON. Black lines depict a linear regression line. DRAGON per-class confidence has smaller dependence on the number of samples in the train.

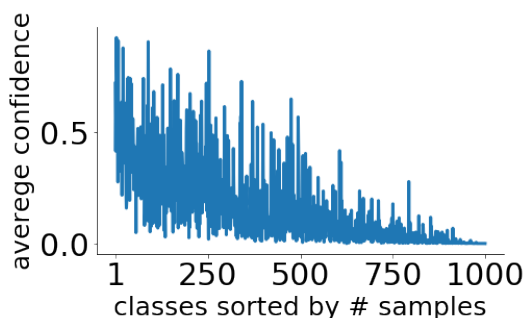


Fig. S 8: The familiarity bias is substantial on ImageNet-LT.

Here we provide a deeper analysis showing that DRAGON effectively addresses the “familiarity bias”.

The familiarity bias causes models to incorrectly favor head classes. Figure 1(d) of the main paper shows the confusion matrix of a standard ResNet-101 trained on long-tail CUB, as computed on the validation set. Classes, of the confusion matrix, are ordered by a decreasing number of training samples, with class #1 having many samples and class #200 have few samples. Black dots denote count larger than 15.

It illustrates two effects. First, the trained model correctly classifies head classes, based on the fact that the top rows have no incorrect (off-diagonal) predictions. Second, for mid and tail classes, predictions are clearly biased towards the head, since there are many more off-diagonal predictions to the left (head class predictions).

DRAGON corrects for the familiarity bias. Figure S7 demonstrates that DRAGON learns to offset some of the familiarity bias. The left panel repeats the curve of Fig 1.b at the main paper, showing the familiarity effect for the visual expert. The right panel shows that DRAGON corrects the familiarity bias and produces a more balanced average confidence across the head and tail classes.

The familiarity bias in large-scale datasets: Figure S8, shows our preliminary analysis for long-tail Imagenet dataset as proposed by [19]. It demonstrates that the familiarity bias is also evident in this large-scale dataset.

B Visual Experts are Better at the Head, Attribute Experts Excel at the Tail

Here we provide supporting evidence to our observation from Section 4 of the main paper: “*Attribute-based models provide relatively accurate predictions in the low-shot regime because a description of a class by its attributes allows to recognize it even when no training samples are available* [16, 37, 3]”. Additionally, we demonstrate that the visual expert is better for the many-shot regime.

We focus on the Two-Level CUB distribution, and evaluate the accuracy for the many shot classes when restricting predictions to these classes (many-among-many), and separately the accuracy for the few-shot classes when predictions are restricted to these tail classes (few-among-few).

Figure S9a shows the accuracy over few-shot classes of both experts in few-among-few setting. The attribute expert outperforms the visual one, and this effect stronger with fewer samples. For example, with 1-shot learning, the attribute expert is almost 100% better than the Visual Expert.

Additionally, when we measure the accuracy of the many-shot classes in the many-among-many setup (accuracy at the head), the visual expert is better than the attribute expert Figure S9b.

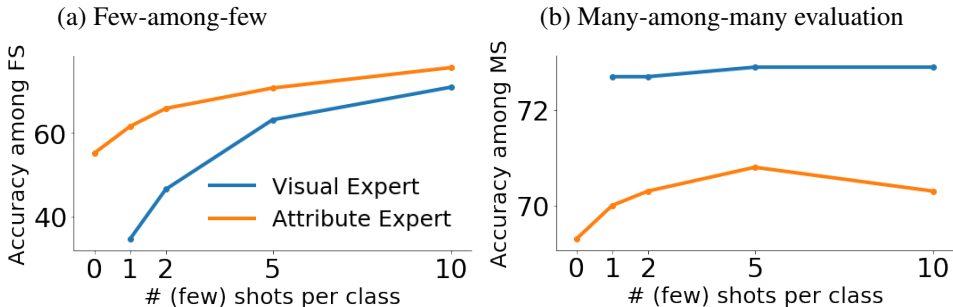


Fig. S 9: Accuracy as a function of number of samples at the tail, of the *Visual Expert* and the *Attribute Expert* used in our study. **(a)** Accuracy among few-shot classes; The attribute expert outperforms the visual expert. **(b)** Accuracy among many-shot classes; The Visual expert outperforms, regardless of the number of samples at the tail.

C More Intuition into the Fusion Architecture

We provide more intuition into the design decisions behind the architecture of the fusion-module.

A major design decision for the fusion architecture stems from the fact that we want the model to perform well at the tail, where very few samples are available per class, as a result, we aimed for a model that has very few parameters.

The fusion-module has two main goals: offset the familiarity bias (predict f_V , f_A) and fuse information from multiple modalities (predict λ). To achieve these, it has to learn to implicitly predict the “richness” of any given sample. Namely, when the model receives a new test sample, it predicts if it is from a head class, a tail class or somewhere between, and adjusts the confidence of the experts accordingly. To do this, it has been shown [2] that profile of confidence values are a good predictor if a sample comes from a head or tail class. Specifically, when considering the softmax output predictions of an expert, the difference between the largest value and the second-largest value can capture information about the confidence of the classifier. More generally, if the softmax outputs are sorted, one can apply a derivative filter over the sorted vector to compute confidence differences, and these carry information about the correctness and confidence of the predictions. We generalize this notion and learn the filter over the sorted output predictions. This is equivalent to learning a one-dimensional ConvNet. Since we have two experts, we further learn a ConvNet with 2×2 filters.

The second key component of the fusion-module is the polynomial model. Here, the model aims to fit a function from the known number of training samples to an offset value, designed to reduce the familiarity bias. While that bias is highly variable across classes, it follows a clear trend. We fit this trend with polynomial because it is very easy to optimize and easily captures monotonic trends. Using the polynomial model, the number of trainable parameters is linear with the number of classes.

| | LONG-TAIL CUB | LONG-TAIL SUN | LONG-TAIL AWA |
|-----------------------------|---------------|---------------|---------------|
| TRAIN # SAMPLES | 2,945 | 4,084 | 6,713 |
| VAL # SAMPLES | 6,495 | 7,388 | 18,210 |
| TEST # SAMPLES | 2,348 | 2,868 | 6,092 |
| TRAIN SET PROPERTIES | | | |
| MAX # SAMPLES | 43 | 12 | 720 |
| MIN # SAMPLES | 3 | 2 | 2 |
| MEAN # SAMPLES | 14.725 | 5.696 | 123.460 |
| MEDIAN # SAMPLES | 11 | 5 | 35 |

Table S 7: Properties of long-tailed CUB, SUN and AWA

At the ablation study (Section 9, main paper) we also tested models where the debiasing factor was learned per-class, regardless of the number of samples, and these models did not perform as well (See Table 3: “non-parametric re-scale”). When learning the debiasing factor per class, the number of trainable parameters is quadratic with the number of classes.

Using the polynomial model, the number of trainable parameters is 1015 with CUB, 3600 with SUN and 265 with AWA. When learning the debiasing factor *per class*, the number of trainable parameters increases to $\sim 80K$ with CUB, $\sim 1M$ with SUN and $\sim 5K$ with AWA.

D Details About the Experimental Setup and Benchmarks

D.1 Constructing Long-tail Evaluation Sets

This section describes how we constructed the *evaluation* set of the long-tail benchmark. It also clarifies a delicate point in Figure 5 of the main paper, where the validation and test splits have a distribution that differs from the train set distribution.

In long-tail learning, the training data follows a non-uniform distribution over classes. For evaluation, there are two different metrics that are most meaningful: First, flat accuracy which is a simple average over per-class accuracy. Second, average over per-class accuracy that agrees with the training distribution.

In both cases, we wish to use all the data that is available. When constructing long-tail distributions from academic benchmarks, one often has to create an unbalanced version of the data since most academic benchmarks are collected in a balanced way. As a result, classes that are assigned to the tail of the distribution, and have few samples in the trainset, may have many leftover samples for evaluation.

To use all available data while keeping a long-tail shape to the distribution of the validation and test sets, we used the following procedure. For each class, we sampled the validation set according to the same long-tail distribution of the training set and computed the accuracy across all classes. We then repeated this process several times and computed the average accuracy, such that all available samples were used for evaluation.

D.2 Properties of our Long-tail Datasets

Table S7 shows the statistics of our benchmark datasets. As described in section 7 of the main paper, we produced long-tail distributions from the original datasets CUB, SUN and AWA following an exponential function to subsample the train set to be long-tail. In all three datasets, tail classes have 2 – 3 samples. We will make the list of samples per-split public upon acceptance.

D.3 A Clarification About the Smooth-Tail Benchmark

In this section, we explain how the long-tail benchmark was aligned with the two-level benchmark, as was mentioned in the paragraph that describes the hold-out subset (Section 6).

To align the long-tail benchmark with the two-level benchmark, we first ordered the classes according to their number of samples in the *two-level* distribution. Then we calculated the number of samples

| Model | Acc_{MS} | Acc_{FS} | Acc_H |
|----------------------|------------------------|------------------------|-------------------------------|
| Most Common Class | 0.7, 0.7, 0.7, 0.7 | 0, 0, 0, 0 | 0, 0, 0, 0 |
| LDAM [6] | 71.5, 71.9, 71.6, 71.5 | 1.2, 5.9, 24.1, 41.2 | 2.4, 10.9, 36.0, 52.2 |
| REVISE [29] | - | - | 36.3, 41.1, 44.6, 50.9 |
| CA-VAE [26] | 58.2, 57.6, 60.0, 62.2 | 44.8, 51.6, 59.4, 62.3 | 50.6, 54.4, 59.6, 62.2 |
| DA-VAE [26] | 50.6, 56.0, 56.8, 56.8 | 47.9, 53.2, 61.0, 65.4 | 49.2, 54.6, 58.8, 60.8 |
| CADA-VAE [26] | 59.6, 60.9, 62.3, 63.1 | 51.4, 57.5, 63.6, 68.8 | 55.2, 59.2, 63.0, 64.9 |
| Visual Expert | 72.7, 72.9, 72.7, 72.0 | 0.6, 3.7, 19.1, 38.6 | 1.2, 6.9, 30.2, 50.2 |
| Attribute Expert | 69.2, 69.0, 69.0, 68.1 | 13.8, 21.9, 38.1, 51.5 | 23.0, 33.2, 49.0, 58.6 |
| DRAGON (ours) | 58.0, 62.9, 63.3, 66.1 | 52.8, 55.9, 63.8, 69.6 | 55.3, 59.2, 63.5, 67.8 |

(a) Two-Level CUB

| Model | Acc_{MS} | Acc_{FS} | Acc_H |
|----------------------|------------------------|------------------------|-------------------------------|
| Most Common Class | 0.2, 0.2, 0.2, 0.2 | 0, 0, 0, 0 | 0, 0, 0, 0 |
| LDAM [6] | 43.7, 44.0, 44.2, 44.3 | 2.2, 6.6, 19.0, 31.8 | 4.3, 11.5, 26.6, 37.0 |
| REVISE [29] | - | - | 27.4, 33.4, 37.4, 40.8 |
| CA-VAE [26] | 35.8, 37.5, 37.5, 39.0 | 40.0, 46.5, 53.8, 55.7 | 37.8, 41.4, 44.2, 45.8 |
| DA-VAE [26] | 34.8, 37.3, 38.6, 38.2 | 41.4, 45.1, 50.2, 54.8 | 37.8, 40.8, 43.6, 45.1 |
| CADA-VAE [26] | 37.6, 38.2, 39.4, 41.9 | 44.1, 49.0, 55.3, 55.1 | 40.6, 43.0, 46.0, 47.6 |
| Visual Expert | 46.3, 46.3, 46.2, 45.6 | 0.9, 4.9, 17.2, 33.0 | 1.8, 8.9, 25.1, 38.3 |
| Attribute Expert | 30.6, 30.4, 30.7, 31.0 | 14.4, 18.7, 21.9, 25.2 | 19.6, 23.2, 25.6, 27.8 |
| DRAGON (ours) | 37.2, 39.2, 40.5, 41.6 | 45.5, 49.6, 55.1, 57.2 | 41.0, 43.8, 46.7, 48.2 |

(b) Two-Level SUN

| Model | Acc_{MS} | Acc_{FS} | Acc_H |
|----------------------|------------------------|------------------------|-------------------------------|
| Most Common Class | 2.5, 2.5, 2.5, 2.5 | 0, 0, 0, 0 | 0, 0, 0, 0 |
| LDAM [6] | 90.7, 90.7, 90.5, 90.5 | 6.6, 14.4, 26.6, 41.6 | 12.4, 24.8, 41.1, 57.0 |
| REVISE [29] | - | - | 56.1, 60.3, 64.1, 67.8 |
| CA-VAE [26] | 73.4, 77.7, 81.0, 81.0 | 56.8, 66.0, 72.8, 77.1 | 64.0, 71.3, 76.6, 79.0 |
| DA-VAE [26] | 74.0, 74.6, 73.5, 73.9 | 63.0, 71.4, 77.7, 79.8 | 68.0, 73.0, 75.6, 76.8 |
| CADA-VAE [26] | 76.6, 79.4, 81.9, 82.6 | 63.8, 68.7, 74.8, 78.0 | 69.6, 73.7, 78.2, 80.2 |
| Visual Expert | 90.7, 90.9, 89.7, 87.9 | 5.9, 11.2, 32.6, 57.9 | |
| Attribute Expert | 82.6, 81.9, 81.7, 81.5 | 11.5, 20.6, 46.2, 59.4 | 20.2, 33.0, 59.0, 68.7 |
| DRAGON (ours) | 74.5, 76.7, 79.2, 81.7 | 61.1, 62.9, 74.3, 82.1 | 67.1, 69.1, 76.7, 81.9 |

(c) Two-Level AWA

Table S 8: Comparing DRAGON with SoTA GFSL models and baselines with increasing number of few-shot training samples on the CUB, SUN and AWA datasets. We report per-class Acc_{MS} , Acc_{FS} and Acc_H . Each cell represents 1-shot,2-shot,5-shot and 10-shot accuracies

| SORTING | Acc_{PC} | Acc_{WGT} | TRAINING PROCESS | Acc_{PC} |
|-----------------------------|-------------|-------------|-----------------------------|-------------|
| NO-SORTING | 56.4 | 57.0 | ALL-TRAIN | 49.5 |
| SORTING-BY-VISUAL-EXPERT | 57.8 | 67.7 | END-TO-END | 41.4 |
| SORTING-BY-ATTRIBUTE-EXPERT | 57.7 | 67.7 | THREE-STAGE-TRAINING | 57.8 |

Table S 9: Results for the ablation study (Section 9) on the *test set* of Smooth-Tail CUB. (Left) The effect of sorting the fusion-module inputs (Section 4.2). (Right) The effect of three-stage training (Section 5).

| MODEL | Acc_{PC} | Acc_{WGT} |
|--|-------------|-------------|
| SIMPLE AVG. | 56.4 | 66.6 |
| F.C. | 56.7 | 66.3 |
| F.C. & $1/n_y$ RE-SCALE | 57.0 | 56.2 |
| F.C. & NON-PARAMETRIC RE-SCALE | 57.0 | 64.3 |
| CONV. & NON-PARAMETRIC RE-SCALE | 56.9 | 67.1 |
| CONV. & SINGLE PARAMETRIC RE-SCALE | 55.8 | 64.3 |
| DRAGON (OURS) (CONV & DUAL PARAMETRIC RE-SCALE) | 57.8 | 67.7 |

Table S 10: Results for the ablation study (Section 9) on the *test-set* of Smooth-Tail CUB for various variants of the fusion-module (Section 4.2). The results show the benefit of using our convolutional backbone and of re-scaling the experts using a parametric mapping.

for each class according to the required long-tail distribution (Section 7 of the main paper), and accordingly drew samples to construct the training set.

D.4 Training CADA on Smooth-Tail Benchmark

In this section, we explain how we trained CADA-VAE [26] for the long-tail benchmark.

To evaluate CADA-VAE [26] on long-tail benchmarks we used the code published by the authors and followed the training protocol exactly as they used for the two-level distribution. Since the protocol relies on a hard distinction between head classes and tail classes, we had to choose where to partition the smooth long-tail distribution to head and tail. Our solution is simple. It is based on the fact that we aligned the order of classes in the long-tail distribution to be the same order as in the two-level split (Section D.3). The alignment allowed us to use the same partition to head and tail as used for the two-level benchmark.

E Additional metrics

E.1 Acc_{FS} and Acc_{MS} on Two-Level Benchmarks

Table S8 provides the results of Acc_{FS} and Acc_{MS} (described in section 8.1) for the Two-Level benchmark. At the main paper we reported the results for the Acc_H metrics, which is derived from Acc_{FS} and Acc_{MS} reported here.

E.2 Ablation Results on the Test Set

In the main paper (Section 9) we described results of ablation study on the validation set. Here we report results for the same model variant on the test set.

Tables S9 and S10 show the results of the ablation study on the test set. It shows the same behavior as the ablation study on the validation set that was reported in the main paper.